PCCP

PAPER

View Article Online
View Journal | View Issue

Cite this: *Phys. Chem. Chem. Phys.*, 2014, **16**, 11901

The first tyrosyl radical intermediate formed in the S_2–S_3 transition of photosystem II†

Marius Retegan, Nicholas Cox, Wolfgang Lubitz, Frank Neese and Dimitrios A. Pantazis*

Received 17th February 2014,
Accepted 3rd April 2014

DOI: 10.1039/c4cp00696h

www.rsc.org/pccp

The EPR "split signals" represent key intermediates of the S-state cycle where the redox active D1-Tyr161 (Y_Z) has been oxidized by the reaction center of the photosystem II enzyme to its tyrosyl radical form, but the successive oxidation of the Mn_4CaO_5 cluster has not yet occurred ($S_iY_Z^\bullet$). Here we focus on the $S_2Y_Z^\bullet$ state, which is formed *en route* to the final metastable state of the catalyst, the S_3 state, the state which immediately precedes O–O bond formation. Quantum chemical calculations demonstrate that both isomeric forms of the S_2 state, the open and closed cubane isomers, can form states with an oxidized $Y_Z^\bullet$ residue without prior deprotonation of the Mn_4CaO_5 cluster. The two forms are expected to lie close in energy and retain the electronic structure and magnetic topology of the corresponding S_2 state of the inorganic core. As expected, tyrosine oxidation results in a proton shift towards His190. Analysis of the electronic rearrangements that occur upon formation of the tyrosyl radical suggests that a likely next step in the catalytic cycle is the deprotonation of a terminal water ligand (W1) of the Mn_4CaO_5 cluster. Diamagnetic metal ion substitution is used in our calculations to obtain the molecular *g*-tensor of $Y_Z^\bullet$. It is known that the g_x value is a sensitive probe not only of the extent of the proton shift between the tyrosine–histidine pair, but also of the polarization environment of the tyrosine, especially about the phenolic oxygen. It is shown for PSII that this environment is determined by the Ca^{2+} ion, which locates two water molecules about the phenoxyl oxygen, indirectly modulating the oxidation potential of Y_Z.

1. Introduction

All oxygenic life on Earth is sustained by biological water oxidation performed in higher plants, algae and cyanobacteria.[1–5] Understanding and mimicking this process in artificial systems is a central challenge for energy research.[6–11] Photosystem II, the enzyme responsible for water splitting, functions by coupling one-electron photochemical charge separation with the four-electron process of water oxidation by storing oxidizing equivalents ("electron holes") on the inorganic Mn_4CaO_5 cluster known as the oxygen evolving complex (OEC), the active site of catalysis. The OEC cycles through five oxidation states S_i, where i = 0–4 indicates the number of stored oxidizing equivalents. S_4 is not observable and spontaneously decays to S_0 with evolution of triplet dioxygen. As shown in Fig. 1, absorption of sunlight by PSII results in charge separation at the reaction center of the enzyme, with the electron being transported through several cofactors to the second exchangeable acceptor, the plastoquinone Q_B. The highly oxidizing radical cation ($P680^{\bullet+}$) is re-reduced by D1-Tyr161 (Y_Z), which subsequently extracts one electron from the Mn_4Ca cluster, advancing it to the next S_i state of the catalytic cycle.

Y_Z oxidation by $P680^{\bullet+}$ occurs on a 1–10 ns timescale. The formed transient radical state ($Y_Z^\bullet$) then decays on the μs to ms timescale, with the concomitant oxidation of the Mn_4CaO_5 cluster under physiological conditions. Cryogenic temperatures (<20 K) alter this single electron progression. At these temperatures, electron donation to $P680^{\bullet+}$ by Y_Z can still occur in a minority of centers (<50%), but the subsequent electron transfer from the Mn_4CaO_5 cluster to $Y_Z^\bullet$ is blocked, arresting catalytic progression from $S_iY_Z^\bullet$ to $S_{i+1}Y_Z$.[12–29] Similar trapped intermediate states can be generated in chemically modified PSII, with examples seen in Ca^{2+} depleted PSII,[30–32] acetate treated PSII,[13,33] and in PSII poised at high pH.[34,35] It is also noted that in the higher S-states (S_2, S_3) infrared light excitation of the Mn_4CaO_5 cluster also allows the "backwards" cycling, *i.e.* inducing the one electron oxidation of Y_Z by the Mn cluster.[15,20,36–38]

From the perspective of electron paramagnetic resonance (EPR) spectroscopy, the tyrosine radical is not isolated from the Mn_4CaO_5 cluster.[39,40] This means that the tyrosyl radical senses the structure of the Mn_4CaO_5 cluster, and hence each metastable $S_iY_Z^\bullet$ state has a characteristic spectral lineshape. Importantly, these "metallo-radical" states have the potential to resolve the

Max Planck Institute for Chemical Energy Conversion, Stiftstr. 34-38, 45470 Mülheim an der Ruhr, Germany. E-mail: dimitrios.pantazis@cec.mpg.de

† Electronic supplementary information (ESI) available. See DOI: 10.1039/c4cp00696h

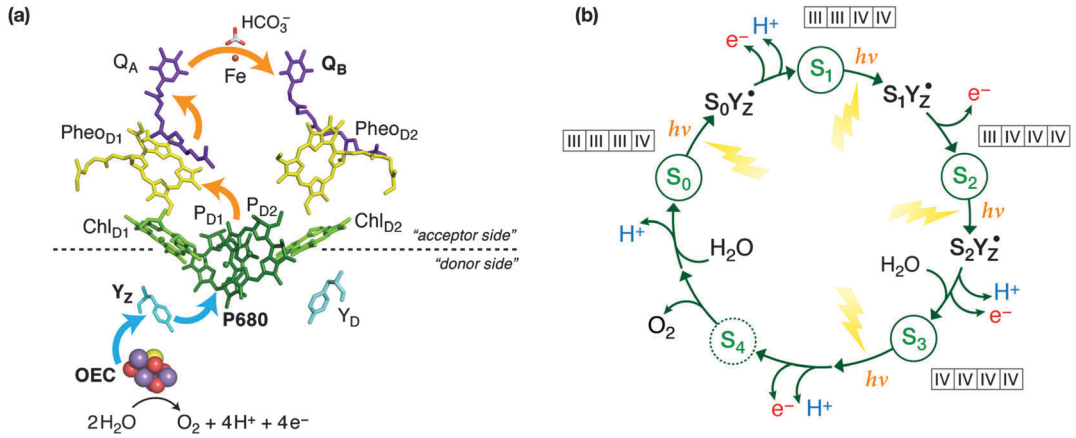

Fig. 1 (a) Schematic depiction of electron flow among the major cofactors of PSII: orange arrows indicate the flow of electrons from P680 after photo-excitation towards the acceptor plastoquinone (Q_B), blue arrows indicate the flow of electrons to P680 from the Mn_4Ca cluster *via* D1-Tyr161 (Y_Z). Water is the ultimate source of electrons, through its oxidation at the OEC. (b) The S-state cycle of the OEC, indicating formation of Y_Z radical intermediates between the first three transitions; the most probable Mn oxidation states are shown for the S_0–S_3 states.

concerted structural changes that occur in-between S-state transitions, which are coupled to cluster deprotonation and substrate binding.[41–45] This is particularly important for the most complicated S-state transition, from S_2 to S_3. While experimental and theoretical efforts have produced a quite robust understanding of the S_2 state itself,[2] the S_3 state is arguably the least well understood state of the cycle, with even the nature of the oxidation event, Mn-centered *vs.* ligand-centered oxidation, still being debated.[46–48] As shown in Fig. 1, S_2–S_3 is a complex transition that must involve several intermediates because it likely combines water binding[43] with deprotonation of the OEC.[41,42] It is the most crucial step of the cycle, because it activates the catalyst allowing the O–O bond formation step to occur. The precise sequence of events within the S_2–S_3 transition is currently unknown and several strands of observations must be rationalized simultaneously for it to be understood.[49]

A quantum chemical description of the electronic structure of the split signal states has been lacking because of (a) the large size of molecular models which must include both the OEC with its first and second coordination spheres and the Y_Z residue with its environment and (b) the sufficiently high levels of theory required to obtain an adequate description of the electronic structure of the coupled system and to predict its spectroscopic properties. In the present work we employ large quantum cluster models to describe the $S_2Y_Z^\bullet$ state. We report its electronic structure and spectroscopic properties, including the *g*-tensor of the tyrosine radical. The present results suggest deprotonation of a terminal water ligand as the most likely next step in the S_2–S_3 transition. We also resolve the influence of hydrogen bonding on the phenolic oxygen of the $Y_Z^\bullet$, suggesting a role for the Ca^{2+} ion in modulating the oxidation potential of the tyrosine by structuring its local hydration environment.

2. Methodology

Optimized models of the S_2 state were used as starting points for geometry optimizations of the one-electron oxidized species.[50] The structures contain all first-sphere residues of the Mn_4CaO_5 core, second-sphere residues that hydrogen-bond to the inorganic core or its first-sphere residues, several vicinal water molecules and the D1-Tyr161–His190 pair, along with complete backbone loops where necessary. The BP86 functional[51,52] was employed for optimizations, while the TPSSh functional[53,54] was used for single-point calculations of different spin configurations in the context of broken-symmetry density functional theory[55–61] and for the calculation of all spectroscopic properties reported in this work. D3 dispersion corrections[62] were used throughout, and the influence of the environment was simulated using the conductor-like screening model (COSMO)[63] assuming a dielectric constant of $\varepsilon = 8$, as in previous studies. The scalar relativistic effects were included with the zeroth order regular approximation (ZORA)[64,65] with one-center terms and using ZORA-recontracted polarized triple-ζ basis sets.[66,67] Fully decontracted auxiliary basis sets were used for the resolution of the identity (RI) and chain-of-spheres (COSX) approximations[68] for the Coulomb and exact exchange, as implemented in ORCA.[69] Fine general integration grids with additionally increased radial accuracy and tight convergence criteria were used for all calculations. The extraction of pairwise exchange coupling constants from the individual broken-symmetry solutions and calculation of the complete energy ladder of spin eigenstates through diagonalization of the Heisenberg Hamiltonian followed established procedures.[50,70–77]

The same level of theory was used for the calculation of the magnetic and spectroscopic parameters. The *g*-matrix describes the coupling between the molecular magnetic moment and the external field. In the framework of DFT and Hartree–Fock theory the *g*-matrix can be evaluated using a coupled-perturbed self-consistent field approach.[78] For the evaluation of the spin–orbit coupling operator we used an efficient implementation of the spin–orbit mean-field approximation to the Breit–Pauli operator.[79] In determining the *g*-matrix components of the Y_Z radical we followed the pragmatic approach of substituting the open-shell Mn ions of the cluster with diamagnetic ions of the same

formal charge (Ga^{3+} and Ge^{4+}), as the interaction between Y_Z and the Mn cluster is small (less than 500 MHz). We note that more elaborate approaches have been proposed for the calculation of *g*-values in magnetically strongly coupled dimers.[80] In the present case, namely the very weak interaction between the hypothetical spin pair, the Y_Z and the Mn cluster, only the electrostatic influence of the inorganic cluster on the tyrosine needs to be considered and can be fully captured using diamagnetic ion substitution.

3. Results and discussion

3.1 The S_2 state prior to the oxidation of Y_Z

The models used in the present work are based on previously optimized models for the S_2 state of the OEC.[50] Recent efforts towards refining the 1.9 Å resolution crystallographic model[81] of PSII for the S_2 state led to the realization that the S_2 state of the cluster can exist in two interconvertible and approximately isoenergetic forms. These two forms of S_2, which can be described as "open cubane" (S_2^A) and "closed cubane" (S_2^B) owing to their core connectivity (see Fig. 2), are valence isomers that differ in the position of the unique Mn(III) ion. This difference in the oxidation state distribution results in distinct magnetic topologies and hence distinct ground spin states for the two structures ($S = 1/2$ for the open cubane and $S = 5/2$ for the closed cubane). These two states correspond to the well-known S_2 state EPR signatures, the $g \approx 2.0$ multiline signal for the open cubane and the $g \approx 4.1$ signal for the closed cubane, with the computed hyperfine coupling constants of the metal ions and the first coordination sphere ligands matching experiment. These two structures also rationalize a series of recent experiments aimed at determining the protonation states of Mn-bound water-derived ligands and identifying one of the substrate oxygen atoms.[2,73,74,76,82–84] The protonation state assignment for the cluster in the S_2 state is as follows: none of the five oxo bridges is protonated (O1–O5) and all four terminal water-derived ligands (W1 and W2 on Mn4, W3 and W4 on Ca^{2+}) represent H_2O ligands, with the exception of W2, which is bound as OH^-.[72]

These experimentally validated models represent a well-defined starting point for the search of the corresponding split signal state. This was initiated by oxidation of the open and closed cubane forms, thus mimicking the first step upon illumination of PSII poised in the S_2 state, *i.e.* the oxidation of Y_Z by $P680^{\bullet+}$. This forms $S_2Y_Z^{\bullet}$, where the tyrosine radical is weakly coupled to the S_2-state Mn cluster (*i.e.* with the same Mn oxidation states as in S_2). As mentioned in the Introduction, this triggers a series of events that results in the formation of the S_3 state, which involves in an unspecified sequence: (i) the reduction of the Y_Z radical by either the last remaining Mn(III) ion of the cluster to yield an all-Mn(IV) configuration or the oxidation of a first coordination sphere ligand; (ii) the binding of the second H_2O substrate molecule; and (iii) the loss of a proton either from the incoming H_2O molecule or from a pre-existing titratable group.

As described in the Introduction, under physiological advancement Y_Z oxidation must occur prior to OEC deprotonation as Y_Z oxidation by $P680^{\bullet+}$ is 2–3 orders of magnitude faster than OEC deprotonation. However, it has been suggested[25] that deprotonation of the Mn cluster may be required to trap/accumulate the $S_2Y_Z^{\bullet}$ intermediate at low temperatures. In this scenario, deprotonation of the cluster presumably serves to retard the decay, *via* charge recombination, of the arrested $S_2Y_Z^{\bullet}$ intermediate. The enhanced lifetime of the $Y_Z^{\bullet}$ state may come about because the lower positive charge of the OEC cluster would stabilize the electron hole on Y_Z. Evidence for this stabilization mechanism is the observation that a pre-illumination of functional PSII samples at elevated temperatures (200 K) increases the subsequent yield of $S_2Y_Z^{\bullet}$ formed at cryogenic (<20 K) temperatures. At this higher temperature the $S_2Y_Z^{\bullet}$ state forms but decays very quickly. Importantly though,

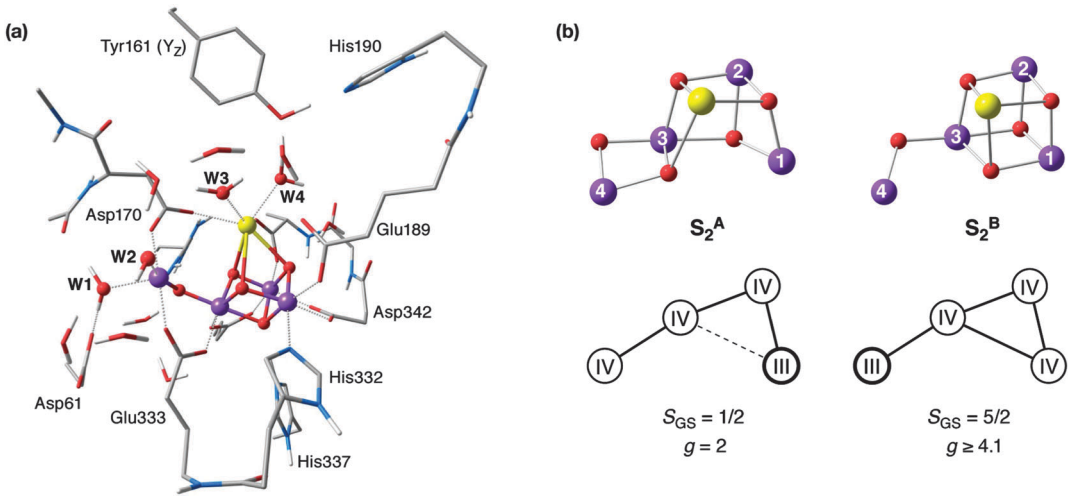

Fig. 2 (a) Model of the OEC including the Y_Z–His190 pair (most of the hydrogen atoms are omitted for clarity). (b) Structure of the S_2 state of the Mn_4CaO_5 core in its two interconvertible forms.

$Y_Z^\bullet$ formation at this temperature is thought to trigger cluster deprotonation, as the protein is flexible enough for proton transfer but not enough to allow S_3 formation, which requires a protein conformational change.[24,30,31,85] While we cannot exclude this possibility, we consider it unlikely. The S_2 state multiline EPR signal is the same with or without this pre-illumination. As demonstrated by Ames *et al.*,[72] deprotonation of the S_2-state cluster should clearly manifest itself in terms of an altered[55] Mn-hyperfine structure, but no such drastic change is observed experimentally. Therefore, we assume that no modification of the OEC needs to occur to trap the first $S_2Y_Z^\bullet$ intermediate state, but instead occurs at a later stage (see Section 3.4).

3.2 Geometric structure of the $S_2Y_Z^\bullet$ states

The optimized open and closed cubane forms of the S_2-state (S_2^A and S_2^B) described above[50] were used as the starting point for optimization of the one-electron oxidized forms. For both structural forms, calculations on the corresponding oxidized species converge to states that contain the Y_Z radical, $S_2^AY_Z^\bullet$ and $S_2^BY_Z^\bullet$. The Mn ions of each structure retain the same electronic configuration and local oxidation states as in the S_2-state models, *i.e.* Mn1 is still a Mn(III) ion in $S_2^AY_Z^\bullet$ and Mn4 is a Mn(III) ion in $S_2^BY_Z^\bullet$. Oxidation of a Mn ion instead of the Y_Z residue was found to be energetically inaccessible. The S_2^A and S_2^B forms were confirmed using multiple computational approaches[50,86] to be very close in energy, less than 2 kcal mol^{-1}; the same is observed here for the $S_2^AY_Z^\bullet$ and $S_2^BY_Z^\bullet$ forms, the latter being 1.3 kcal mol^{-1} higher in energy than the former for the BP86 optimized structures.

As the manganese ions do not change their electronic state, the geometric changes observed upon Y_Z oxidation are insignificant in the region of the inorganic core. However, this is not the case for Y_Z. In the $S_2^AY_Z^\bullet$ model, the tyrosine loses the proton (the O–H distance is 1.639 Å compared to 1.096 Å in the S_2^A state), which shifts spontaneously to the τ-N (N_ε) atom of the imidazole ring of His190 (N–H = 1.058 Å *vs.* 1.439 Å in S_2^A). Similar changes are observed in the $S_2^BY_Z^\bullet$ form, where the O–H and N–H distances are 1.592 and 1.067 Å, respectively, compared with 1.109 and 1.412 in the S_2^B state. This proton shift suggests that the tyrosyl in $S_2Y_Z^\bullet$ is best described as a neutral radical coupled to an imidazolium cation. It is noted that such a proton transfer was proposed for the D2-Tyr160 (Y_D) radical (to D2-His189),[87,88] but a recent work of Saito *et al.* instead suggested that the proton acceptor partner for the homologous Y_D residue is a nearby water molecule, explaining why its oxidation is not reversible.[89] This same proton shift has been demonstrated in biomimetic model systems.[90,125]

3.3 Electronic structure of the $S_2Y_Z^\bullet$ states

Fig. 3(a) shows the frontier spin-α and spin-β orbitals of the S_2 state of the OEC in the multiline $g \approx 2$ (S_2^A) conformation. For both spin manifolds, the HOMO − 1 is a π-type orbital localized

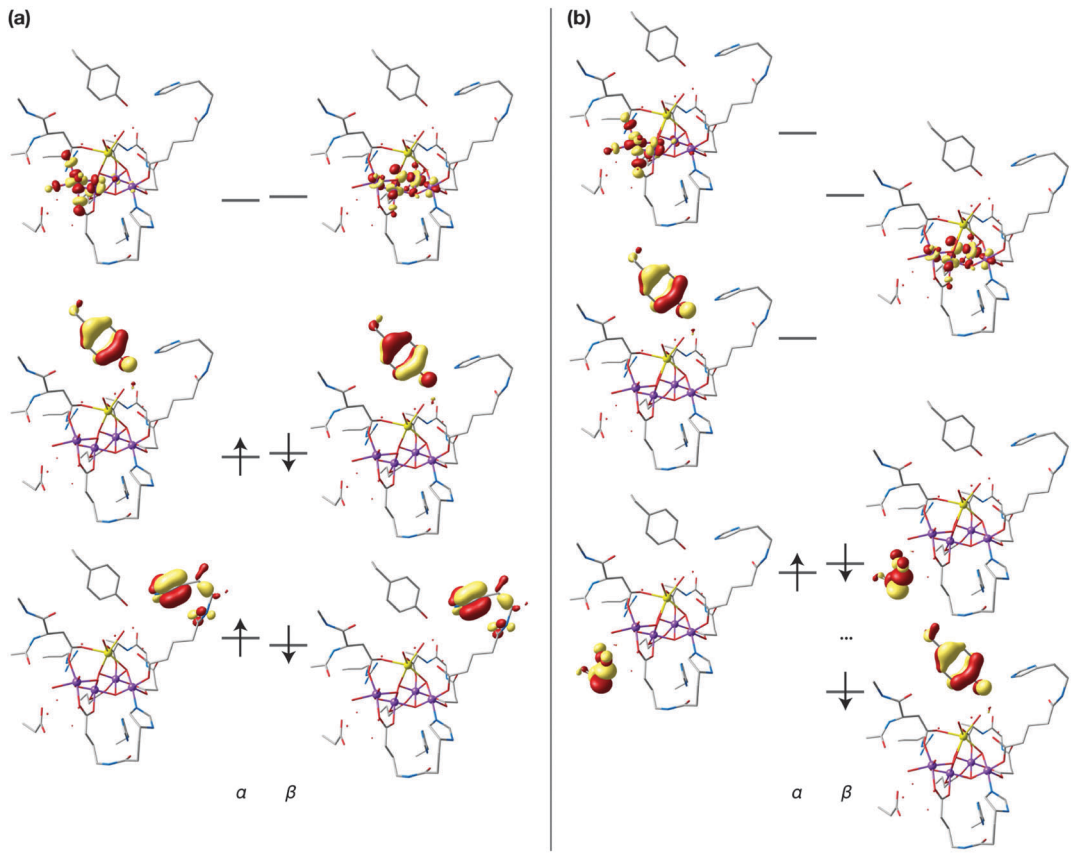

Fig. 3 Frontier orbitals of the S_2^A model of the OEC (a) and the oxidized $S_2^AY_Z^\bullet$ model (b); hydrogen atoms are omitted for clarity.

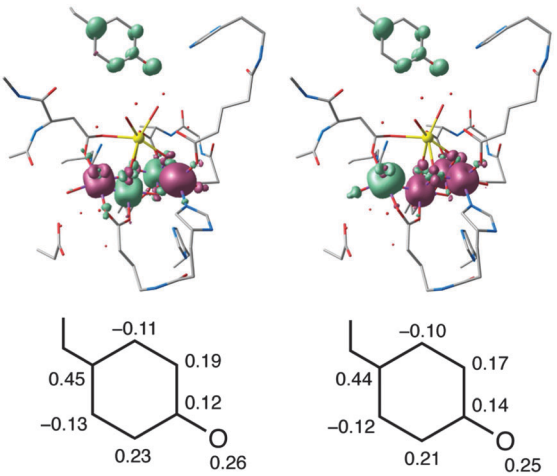

Fig. 4 Spin density maps and Mulliken spin populations on the tyrosyl fragment for models of the open cubane $S_2^AY_Z^\bullet$ (left) and closed cubane $S_2^BY_Z^\bullet$ (right) states of the OEC in their respective lowest-energy broken-symmetry spin configurations.

mostly on the imidazole ring of His190 and the HOMO is localized on Tyr161. This orbital takes the form of an anti-bonding combination of the second-lowest occupied π orbital of the benzyl ring with the p_π orbital of the oxygen atom. All dominantly manganese-based orbitals lie lower in energy. The LUMOs are different for the two manifolds: the α-LUMO is a metal–ligand σ-antibonding orbital localized on Mn4 whereas the β-LUMO is exclusively of metal character, being almost equally distributed over Mn2, Mn3 and Mn4. A similar configuration is obtained for the closed cubane form S_2^B (see ESI†). In the context of this one-particle picture, the tyrosine-based HOMO should be the orbital involved in the one-electron oxidation of the system. This is precisely what the calculations on the $S_2Y_Z^\bullet$ states demonstrate: Fig. 3(b) depicts the frontier orbitals of the oxidized $S_2^AY_Z^\bullet$ state (for the corresponding orbitals of $S_2^BY_Z^\bullet$, see the ESI†), while Fig. 4 shows the spin density distributions for both forms of the cluster with a clear localization of the π-type unpaired spin density on the phenoxyl ring. The spin populations are also consistent with the localization of one unpaired electron on Y_Z; as in the S_2 state, the spin populations on the Mn ions are close to the values expected for the formal oxidation states of III and IV, *ca.* 3.8–3.9 and 2.9–3.0 unpaired electrons, respectively.

It is stressed that no valence isomers could be found where the Mn(III) ion is oxidized instead of Y_Z. This suggests that the S_2 state cannot proceed to the S_3 state but instead is arrested in the $S_2Y_Z^\bullet$ state. It is also important to note that the S_2 state structures were developed using backbone constraints from X-ray crystallographic data and are fully consistent with the EPR results which constrain the protonation state. Thus our results require a conformational change during the S_2 to S_3 transition to allow the oxidation of the cluster, in line with earlier experimental results. It is noted that if the Tyr161–His190 pair is absent from the S_2 state model, the HOMO is fundamentally different by construction from the one described above. Oxidation of such an S_2-state model without further modifications

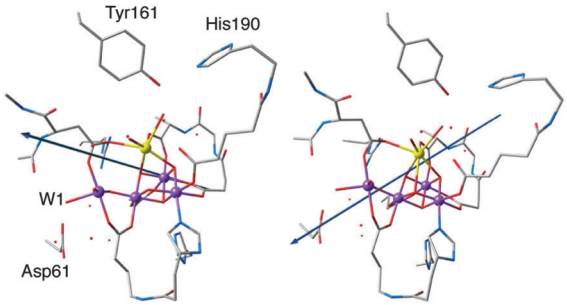

Fig. 5 Dipole moment in the S_2^B state (left) and in the oxidized $S_2^BY_Z^\bullet$ state (right).

(water binding and/or deprotonation) leads, by definition, to an "unphysical" oxidation event that cannot have any correspondence to the natural system.

3.4 Y_Z oxidation reorients the dipole moment of the OEC

An important question regarding the mechanistic details of the S_2–S_3 transition is what happens after the oxidation of Y_Z by $P680^{\bullet+}$ and the formation of $S_2Y_Z^\bullet$. Although the next steps are not explicitly studied in the present work, an important observation is that the dipole moment of the model is reoriented after Y_Z oxidation. Fig. 5 compares the dipole moment vector before and after oxidation of Y_Z. It can be seen that in the "split signal" state the dipole moment is directed in such a way that it points approximately from the cationic imidazolium of His190 to Asp61. The same result is seen for both $S_2^AY_Z^\bullet$ and $S_2^BY_Z^\bullet$, suggesting that this region of the OEC is now the locus of the negative charge regardless of the formal oxidation state of Mn4.

In the context of the putative requirements for progression to the S_3 state (see Fig. 1), this dipole reorientation can be interpreted as indicating the likely direction of proton removal from the system. Given that the dipole is almost coincident with the Mn4–W1 bond and Asp61, it is likely that Y_Z oxidation triggers the loss of a proton from W1 to the acceptor Asp61. This was suggested also in previous computational studies[91–93] and would be consistent with the proposal that: (i) proton release occurs prior to formation of the S_3 state[42] and (ii) Asp61 participates in a proton-transfer pathway involving the proximal chloride ion.[94–97] Note that a continuous network of hydrogen bonds formed by a chain of water molecules between Y_Z and Mn4 establishes a communication pathway across the cluster.[89,98–101]

3.5 Magnetism of the $S_2Y_Z^\bullet$ states

The magnetism of each $S_2Y_Z^\bullet$ model is defined by Mn–Mn ion exchange interactions within the inorganic cluster, and the tyrosine–OEC interaction which is orders of magnitude smaller. For the two configurations discussed above ($S_2^AY_Z^\bullet$ and $S_2^BY_Z^\bullet$) an overdetermined system of equations, which is derived from the set of broken-symmetry solutions, can be solved by singular value decomposition to yield pairwise exchange coupling constants, J_{ij}, shown in Fig. 6. Based on these values, diagonalization of the Heisenberg Hamiltonian then yields the complete spectrum of energy levels produced by the coupling of the four

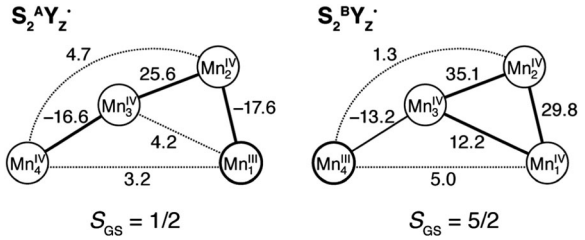

Fig. 6 Exchange coupling constants (cm^{-1}) and ground spin states of the Mn_4CaO_5 subunit for the open-cubane (left) and closed-cubane (right) forms of the $S_2Y_Z^\bullet$ state.

local spins of each model. In line with the small structural perturbations of the inorganic core upon Y_Z oxidation, the exchange coupling constants for the $S_2{}^AY_Z^\bullet$ and $S_2{}^BY_Z^\bullet$ models are similar to those obtained previously for the corresponding S_2 state models: in the open cubane form there are two antiferromagnetic couplings, between Mn1–Mn2 and Mn3–Mn4, whereas in the closed cubane form all interactions within the cuboidal part are ferromagnetic.[50,75]

These results require that the two clusters retain the same ground spin state seen in the corresponding S_2 state structure, *i.e.* $S = 1/2$ for the open cubane and $S = 5/2$ for the closed cubane form. The first excited states and their separation are also similar: $S = 3/2$ at 23.2 cm^{-1} and $S = 7/2$ at 8.6 cm^{-1}, respectively. In view of these results, it can be surmised that the split signals arising from the $S_2{}^AY_Z^\bullet$ and $S_2{}^BY_Z^\bullet$ forms reflect the interaction of the $S = 1/2$ tyrosyl radical with the OEC exhibiting a net spin state of different magnitudes in each case. As the two oxidized forms remain as close in energy as in S_2, it might be expected that illumination of PSII poised in the S_2 state with both $S_2{}^A$ and $S_2{}^B$ forms being populated, would lead to formation of both $S_2{}^AY_Z^\bullet$ and $S_2{}^BY_Z^\bullet$, and therefore of two split signals. However, only a signal attributed to an interaction of $Y_Z^\bullet$ with a spin 1/2 state of the manganese cluster has been experimentally observed. The above results do not allow us to address the question why the putative $S_2{}^BY_Z^\bullet$ split signal has not yet been observed, since the present calculations reveal nothing about the lifetimes of the states or their possible decay pathways. Nevertheless, the results allow us to positively identify the experimentally observed split signal of the S_2 state with the open cubane conformation of the manganese cluster, *i.e.* with the $S_2{}^AY_Z^\bullet$ model. It is noted though that the closed cubane conformation may be associated with the NIR-induced split signals (see Introduction).

Turning now to the coupling between the inorganic cluster and the oxidized tyrosine, according to simulations of EPR spectra, this interaction is of the order of −400 MHz.[13] Since this value is very small, it becomes important to eliminate all numerical noise from the calculations and for this reason a higher threshold for convergence was used for the computed broken-symmetry energies. Nevertheless, when confronted with such energy differences, agreement of the calculation with experiment even in terms of the order of magnitude should be considered satisfactory. In the present case the calculated values for the coupling of $Y_Z^\bullet$ with the manganese cluster are −819 MHz for $S_2{}^AY_Z^\bullet$ and −626 MHz for $S_2{}^BY_Z^\bullet$, when the lowest-energy spin configuration is used in the broken-symmetry calculations for each of the manganese clusters ($|\alpha\beta\beta\alpha>$, $M_S = 1/2$ for the open cubane and $|\alpha\alpha\alpha\beta>$, $M_S = 5/2$ for the closed cubane form). If instead the high-spin ($M_S = 13/2$) configuration of the clusters is used, then the corresponding values become −149 MHz for $S_2{}^AY_Z^\bullet$ and −324 MHz for $S_2{}^BY_Z^\bullet$. In either case the models used in this work correctly capture the essential physics of the interaction.

3.6 The *g*-matrix of the $Y_Z^\bullet$ radical

The calculation of the *g*-matrix in tyrosine radicals has been attempted previously using various approaches. The majority of these initial studies used simplified models such as the phenoxyl–water or phenoxyl–imidazolium pair to obtain structural and spectroscopic properties of the tyrosine radical.[102–108] Recently, more elaborate models of PSII that include the surrounding residues were used to study the histidine–tyrosine pair for both Y_Z and Y_D.[88,89,109,110] In addition to considering the effects of the protein on the calculated properties, these larger models have allowed the environment of the two redox active tyrosine residues of PSII (Y_D and Y_Z) to be differentiated.

Our *g*-matrix calculations match earlier model system studies regarding the *g* orientation with respect to the phenoxyl ring: the g_x axis is oriented almost perfectly along the C–O bond ($\theta = 3.8^\circ$) and g_z is perpendicular to the plane of the ring (Fig. 7). The values of the individual *g*-matrix components are identical for the two forms of the cluster, indicating the absence of any effect derived from the different magnetic topologies of the inorganic core.

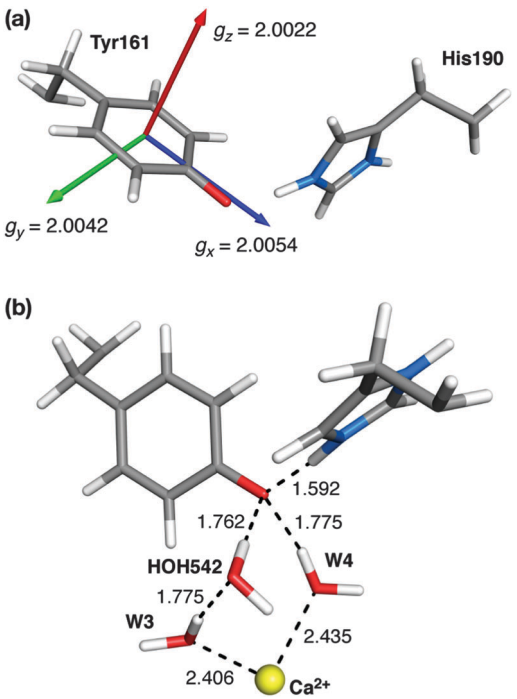

Fig. 7 (a) Orientation and components of the *g*-matrix for the $S_2{}^BY_Z^\bullet$ state. (b) Water molecules involved in hydrogen bonding to $Y_Z^\bullet$ (distances, in Å, shown for the $S_2{}^BY_Z^\bullet$ model).

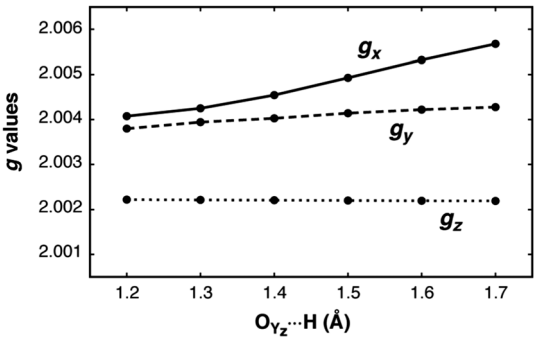

Fig. 8 Scan of the g values for the $S_2{}^{B}Y_Z^{\bullet}$ model with respect to the $Y_Z^{\bullet}O\cdots H$ distance.

The dependence of the g-matrix elements on the position of the proton between the Y_Z–His190 pair is depicted in Fig. 8. The g_x component shows the strongest dependence: the largest calculated value corresponds to the largest O···H distance (g_x = 2.0057), while the smallest value is obtained for the structure in which the hydrogen is closest to the oxygen atom of the $Y_Z^{\bullet}$ radical (g_x = 2.0041). For the g_y and g_z components no such dependence is observed, in agreement with the previous tyrosyl radical g-tensor studies.

EPR studies of $Y_Z^{\bullet}$ have been performed by replacing Y_D by phenylalanine and removing the Mn cluster (see ref. 39 and references therein for a review of the relevant literature). In contrast to $Y_D^{\bullet}$, the g-matrix anisotropy of Y_Z (in the absence of the OEC cluster) has only recently been measured.[108] The values of g_x = 2.00714 in frozen solution and 2.00705 in single crystals have been reported,[108] while the experimental values of g_y and g_z match the computed ones of Fig. 7a almost exactly. These higher values of g_x are similar to the ones reported for the much more extensively studied Tyr160 (Y_D) of the D2 protein of PSII; a compilation of $Y_D^{\bullet}$ values for different organisms is given in Hofbauer *et al.* ($g_x \approx$ 2.0074–2.0078).[111] Compared with these values and those of other systems, the computed value of 2.0054 for g_x appears to be somewhat small. However, g_x is known to strongly depend on hydrogen bonding and the local electrostatic interactions. To give a few representative examples, the g_x value of the tyrosyl radical $Y_{122}^{\bullet}$ in *E. coli* ribonucleotide reductase (RNR) shifts from 2.0087 to 2.0091 in the absence of any hydrogen bonding to *ca.* 2.0076 in a more polar environment,[104,112,113] similar to the value for the $Y_D^{\bullet}$ of PSII. At the other extreme, a value of g_x = 2.0052 for the $NH_2Y_{730}^{\bullet}$ radical in *E. coli* RNR has been observed,[114] resulting from the combined influence of three hydrogen bonds.[115] Similarly, in phenoxyl radical compounds that contain a strong intramolecular hydrogen bond the g_x values fall within 2.0063–2.0067.[116] In the present case the low g_x value of 2.0054 for $S_2Y_Z^{\bullet}$ can be interpreted as being due to the existence of three hydrogen-bonding interactions, two from adjacent water molecules (see Fig. 7b) and one from the proton that shifts to the imidazole of His190, which remains at a distance of approximately 1.6 Å from the O atom of $Y_Z^{\bullet}$.

To test this hypothesis, three additional calculations were carried out on fragments of the full model. First, the inorganic part of the model and all its associated ligands were removed, leaving a model containing only the Y_Z–His190 pair and the two water molecules that form direct hydrogen bonds to the phenoxyl oxygen, the calcium-bound W4 (HOH540 in the 3ARC PDB structure) and the HOH542 that forms a hydrogen-bonding bridge between the other calcium-bound water (W3 or HOH541) and the tyrosine. The structure was not allowed to relax, essentially isolating the effect of the inorganic cluster while retaining the immediate environment of the tyrosine. As shown in Table 1, the effect of the Mn cluster on the low g_x value is insignificant. Removing also the HOH542 molecule results in an increase of g_x value to 2.0063. However, the largest effect was observed when both H-bonding water molecules were removed; the model that contains only the two amino acid residues displays a marked increase in the g_x value to 2.0072, showing how the local electropositive environment plays a crucial role in suppressing the expected effect on g_x of the proton shift to His190.

Table 1 Components of the g-matrix and the total atomic spin population of the oxygen atom computed with models of different sizes

Model	g_x	g_y	g_z	ρ_O
Full model	2.0054	2.0042	2.0022	0.254
$Y_Z^{\bullet}$–His with W4, HOH542	2.0055	2.0043	2.0023	0.267
$Y_Z^{\bullet}$–His with W4	2.0063	2.0044	2.0022	0.321
$Y_Z^{\bullet}$–His	2.0072	2.0046	2.0022	0.360

As demonstrated previously for a series of synthetic phenoxyl radical models, the value of g_x tracks closely the change in the unpaired spin population on the oxygen atom (Table 1 and Fig. S3, ESI†), the atom with the largest spin–orbit coupling constant.[116] An almost linear correlation is observed between the O spin population and g_x, with R^2 = 0.993. The change in spin population can be interpreted as the result of increased hydrogen bonding "pulling" the electron density towards the oxygen and hence "pushing" the unpaired density over the phenyl ring, an effect also seen for the in-plane proton alone (Fig. 8). A detailed discussion of this effect is provided by Sinnecker *et al.* for hydrogen bonding in semiquinones[117] and for the case of the primary quinone ($Q_A/Q_A^{\bullet -}$) in bacterial reaction centers.[118]

It is noted that the larger value of g_x for the model where the hydrogen-bonded water molecules are removed agrees with the experimental value reported for $Y_Z^{\bullet}$ in Mn-depleted PSII and with that reported for the Y_D radical. The above observation regarding g_x implies that the removal of the OEC cluster in the experiments also perturbs the native hydration environment of Y_Z. As a corollary, and given the highly ordered hydrogen bonding network shown in Fig. 7, it can be suggested that in addition to other roles,[3,119–121] the Ca^{2+} ion serves to structure the water molecules in that region and adjust their acidities in order to (a) modulate the electronic structure and hence the redox potential of the tyrosine residue and (b) optimize the hydrogen-bond-mediated communication between Y_Z and the inorganic cluster.

Given that the hydrogen bonding network into which Y_Z is embedded must be highly optimized for a proper function, even small perturbations on the structure and pK_A value of the constituent water molecules may have a significant impact on the function of the catalyst. The role of the structured water environment in modulating the redox potential of the tyrosyl

radical can be inferred by estimating the electron affinities of the simplified models of Table 1. DFT calculations suggest that the absence or presence of the water molecules at the optimized positions shifts the electron affinity by *ca.* 0.46/0.28 eV (vertical/adiabatic values; Fig. S4, ESI†). The above suggestion for the role of the Ca^{2+} ion is consistent with the measurements of frequency shifts of the proximal peptide carbonyl bands as markers for hydrogen-bonding changes between the S_1–S_2 transition in the presence of different cations.[122] It is also in line with the recent proposal of Boussac and coworkers regarding the Ca^{2+} ion acting as an entropic regulator for the S_3–S_0 transition based on its involvement in structuring the environment of Y_Z in the S_3 state.[123]

4. Conclusions

In this work we developed structural models for the $S_2Y_Z^{\bullet}$ "split signal" state of the OEC, based on the open-cubane (S_2^A) and closed-cubane (S_2^B) forms of the S_2 state. It was observed that no proton removal was required to form the oxidized states $S_2^AY_Z^{\bullet}$ and $S_2^BY_Z^{\bullet}$. In addition, no valence isomers could be found where the Mn(III) ion is oxidized instead of Y_Z, implying that a chemical modification of the OEC is necessary for the subsequent S_2 to S_3 transition to occur. The reorientation of the dipole moment suggests that this most probably involves the deprotonation of W1.

The calculations of the tyrosyl *g*-matrix provide estimates (g_x = 2.0054, g_y = 2.0042, and g_z = 2.0022) that form a good predictive basis regarding the environment of the tyrosine. The response of the *g*-matrix components was examined with respect to the extent of proton transfer to the τ-N of His190 and the contribution of different subsets of the model. The predicted g_x value is due to the presence of three hydrogen bonding interactions in which calcium-bound water molecules are involved. Given that the existing experimental *g*-anisotropy values were obtained from measurements on Ca-depleted PSII samples, it is suggested that the measured values do not necessarily reflect the natural environment of Y_Z because they presumably miss the structuring effect of the Ca^{2+} ion which operates in the native system. Thus, the Ca^{2+} ion, besides its possible role in adjusting the redox potential of the inorganic cluster itself, as also indicated in studies of synthetic complexes,[124] has an additional role; it organizes the water environment and optimizes the hydrogen-bonding network around Y_Z. Since, as demonstrated by the present results, hydrogen bonding to W4 and HOH542 strongly affects the electronic structure of the tyrosyl radical through modulation of its spin and charge density distribution, this ordering effect of the Ca^{2+} ion indirectly fine-tunes the function of the tyrosine residue by regulating its redox potential and electron transfer properties.

References

1 J. Messinger and G. Renger, in *Primary Processes of Photosynthesis, Part 2: Principles and Apparatus*, The Royal Society of Chemistry, Cambridge, 2008, vol. 9, pp. 291–349.
2 N. Cox, D. A. Pantazis, F. Neese and W. Lubitz, *Acc. Chem. Res.*, 2013, **46**, 1588–1596.
3 J. P. McEvoy and G. W. Brudvig, *Chem. Rev.*, 2006, **106**, 4455–4483.
4 R. E. Blankenship, *Molecular Mechanisms of Photosynthesis*, Blackwell, Oxford, 2001.
5 N. Cox and W. Lubitz, in *Chemical Energy Storage*, ed. R. Schlögl, De Gruyter, Berlin, 2013, pp. 185–224.
6 S. DeBeer, M. van Gastel, E. Bill, S. Ye, T. Petrenko, D. A. Pantazis and F. Neese, in *Chemical Energy Storage*, ed. R. Schlögl, De Gruyter, Berlin, 2013, pp. 353–377.
7 H. Dau, C. Limberg, T. Reier, M. Risch, S. Roggan and P. Strasser, *ChemCatChem*, 2010, **2**, 724–761.
8 J. Barber, *Chem. Soc. Rev.*, 2009, **38**, 185–196.
9 W. Lubitz, E. J. Reijerse and J. Messinger, *Energy Environ. Sci.*, 2008, **1**, 15–31.
10 M. M. Najafpour, A. N. Moghaddam, S. I. Allakhverdiev and Govindjee, *Biochim. Biophys. Acta, Bioenerg.*, 2012, **1817**, 1110–1121.
11 D. G. Nocera, *Acc. Chem. Res.*, 2012, **45**, 767–776.
12 V. Petrouleas, D. Koulougliotis and N. Ioannidis, *Biochemistry*, 2005, **44**, 6723–6728.
13 J. M. Peloquin, K. A. Campbell and R. D. Britt, *J. Am. Chem. Soc.*, 1998, **120**, 6840–6841.
14 J. H. A. Nugent, I. P. Muhiuddin and M. C. W. Evans, *Biochemistry*, 2002, **41**, 4117–4126.
15 N. Ioannidis and V. Petrouleas, *Biochemistry*, 2000, **39**, 5246–5254.
16 C. Zhang and S. Styring, *Biochemistry*, 2003, **42**, 8066–8076.
17 C. Zhang, A. Boussac and A. W. Rutherford, *Biochemistry*, 2004, **43**, 13787–13795.
18 K. G. V. Havelius, J.-H. Su, Y. Feyziyev, F. Mamedov and S. Styring, *Biochemistry*, 2006, **45**, 9279–9290.
19 N. Ioannidis, G. Zahariou and V. Petrouleas, *Biochemistry*, 2006, **45**, 6252–6259.
20 J.-H. Su, K. G. V. Havelius, F. M. Ho, G. Han, F. Mamedov and S. Styring, *Biochemistry*, 2007, **46**, 10703–10712.
21 A. Boussac, M. Sugiura, T.-L. Lai and A. W. Rutherford, *Philos. Trans. R. Soc., B*, 2008, **363**, 1203–1210.
22 G. Sioros, D. Koulougliotis, G. Karapanagos and V. Petrouleas, *Biochemistry*, 2006, **46**, 210–217.
23 M. Chrysina, G. Zahariou, N. Ioannidis and V. Petrouleas, *Biochim. Biophys. Acta, Bioenerg.*, 2010, **1797**, 487–493.
24 M. Chrysina, G. Zahariou, Y. Sanakis, N. Ioannidis and V. Petrouleas, *J. Photochem. Photobiol., B*, 2011, **104**, 72–79.
25 J. Sjöholm, S. Styring, K. G. V. Havelius and F. M. Ho, *Biochemistry*, 2012, **51**, 2054–2064.
26 J.-H. Su, K. G. V. Havelius, F. Mamedov, F. M. Ho and S. Styring, *Biochemistry*, 2006, **45**, 7617–7627.
27 N. Cox, F. M. Ho, N. Pewnim, R. Steffen, P. J. Smith, K. G. V. Havelius, J. L. Hughes, L. Debono, S. Styring, E. Krausz and R. J. Pace, *Biochim. Biophys. Acta, Bioenerg.*, 2009, **1787**, 882–889.
28 K. G. V. Havelius, J.-H. Su, G. Han, F. Mamedov, F. M. Ho and S. Styring, *Biochim. Biophys. Acta, Bioenerg.*, 2011, **1807**, 11–21.
29 K. G. V. Havelius, J. Sjöholm, F. Ho, F. Mamedov and S. Styring, *Appl. Magn. Reson.*, 2010, **37**, 151–176.

30 A. Boussac and A. W. Rutherford, *Biochemistry*, 1988, **27**, 3476–3483.
31 A. Boussac, J. L. Zimmermann and A. W. Rutherford, *Biochemistry*, 1989, **28**, 8984–8989.
32 M. Sivaraja, J. Tso and G. C. Dismukes, *Biochemistry*, 1989, **28**, 9459–9464.
33 D. A. Force, D. W. Randall and R. D. Britt, *Biochemistry*, 1997, **36**, 12062–12070.
34 P. Geijer, F. Morvaridi and S. Styring, *Biochemistry*, 2001, **40**, 10881–10891.
35 J. Sjöholm, K. G. V. Havelius, F. Mamedov and S. Styring, *Biochemistry*, 2010, **49**, 9800–9808.
36 N. Ioannidis, J. H. A. Nugent and V. Petrouleas, *Biochemistry*, 2002, **41**, 9589–9600.
37 N. Ioannidis and V. Petrouleas, *Biochemistry*, 2002, **41**, 9580–9588.
38 D. Koulougliotis, J.-R. Shen, N. Ioannidis and V. Petrouleas, *Biochemistry*, 2003, **42**, 3045–3053.
39 W. Lubitz, in *Electron Paramagnetic Resonance*, ed. B. C. Gilbert, M. J. Davies and D. M. Murphy, The Royal Society of Chemistry, 2004, vol. 19, pp. 174–242.
40 A. Haddy, *Photosynth. Res.*, 2007, **92**, 357–368.
41 H. Dau and M. Haumann, *Biochim. Biophys. Acta, Bioenerg.*, 2007, **1767**, 472–483.
42 A. Klauss, M. Haumann and H. Dau, *Proc. Natl. Acad. Sci. U. S. A.*, 2012, **109**, 16035–16040.
43 T. Noguchi, *Philos. Trans. R. Soc., B*, 2008, **363**, 1189–1195.
44 J. Messinger, T. Noguchi and J. Yano, in *Molecular Solar Fuels*, ed. T. J. Wydrzynski and W. Hillier, The Royal Society of Chemistry, Cambridge, 2012, pp. 163–207.
45 W. Hillier and T. Wydrzynski, *Coord. Chem. Rev.*, 2008, **252**, 306–317.
46 J. Messinger, J. H. Robblee, U. Bergmann, C. Fernandez, P. Glatzel, H. Visser, R. M. Cinco, K. L. McFarlane, E. Bellacchio, S. A. Pizarro, S. P. Cramer, K. Sauer, M. P. Klein and V. K. Yachandra, *J. Am. Chem. Soc.*, 2001, **123**, 7804–7820.
47 M. Haumann, C. Müller, P. Liebisch, L. Iuzzolino, J. Dittmer, M. Grabolle, T. Neisius, W. Meyer-Klaucke and H. Dau, *Biochemistry*, 2005, **44**, 1894–1908.
48 P. Glatzel, H. Schroeder, Y. Pushkar, T. Boron, S. Mukherjee, G. Christou, V. L. Pecoraro, J. Messinger, V. K. Yachandra, U. Bergmann and J. Yano, *Inorg. Chem.*, 2013, **52**, 5642–5644.
49 N. Cox and J. Messinger, *Biochim. Biophys. Acta, Bioenerg.*, 2013, **1827**, 1020–1030.
50 D. A. Pantazis, W. Ames, N. Cox, W. Lubitz and F. Neese, *Angew. Chem., Int. Ed.*, 2012, **51**, 9935–9940.
51 J. P. Perdew, *Phys. Rev. B: Condens. Matter Mater. Phys.*, 1986, **33**, 8822–8824.
52 A. D. Becke, *Phys. Rev. A*, 1988, **38**, 3098–3100.
53 V. N. Staroverov, G. E. Scuseria, J. Tao and J. P. Perdew, *J. Chem. Phys.*, 2003, **119**, 12129–12137.
54 J. Tao, J. P. Perdew, V. N. Staroverov and G. E. Scuseria, *Phys. Rev. Lett.*, 2003, **91**, 146401.
55 L. Noodleman, *J. Chem. Phys.*, 1981, **74**, 5737–5743.
56 K. Yamaguchi, Y. Takahara and T. Fueno, in *Applied Quantum Chemistry*, ed. V. H. Smith Jr., H. F. Schaefer III, K. Morokuma and D. Reidel, Boston, 1986, p. 155.
57 S. Yamanaka, T. Kawakami, H. Nagao and K. Yamaguchi, *Chem. Phys. Lett.*, 1994, **231**, 25–33.
58 A. Bencini, F. Totti, C. A. Daul, K. Doclo, P. Fantucci and V. Barone, *Inorg. Chem.*, 1997, **36**, 5022–5030.
59 F. Neese, *Coord. Chem. Rev.*, 2009, **253**, 526–563.
60 M. Orio, D. A. Pantazis and F. Neese, *Photosynth. Res.*, 2009, **102**, 443–453.
61 F. Neese, W. Ames, G. Christian, M. Kampa, D. G. Liakos, D. A. Pantazis, M. Roemelt, P. Surawatanawong and S. F. Ye, *Adv. Inorg. Chem.*, 2010, **62**, 301–349.
62 S. Grimme, J. Antony, S. Ehrlich and H. Krieg, *J. Chem. Phys.*, 2010, **132**, 154104–154119.
63 A. Klamt and D. Schüürman, *J. Chem. Soc., Perkin Trans. 2*, 1993, 799–805.
64 E. van Lenthe, E. J. Baerends and J. G. Snijders, *J. Chem. Phys.*, 1994, **101**, 9783–9792.
65 E. van Lenthe, J. G. Snijders and E. J. Baerends, *J. Chem. Phys.*, 1996, **105**, 6505–6516.
66 D. A. Pantazis, X. Y. Chen, C. R. Landis and F. Neese, *J. Chem. Theory Comput.*, 2008, **4**, 908–919.
67 A. Schäfer, C. Huber and R. Ahlrichs, *J. Chem. Phys.*, 1994, **100**, 5829–5835.
68 F. Neese, F. Wennmohs, A. Hansen and U. Becker, *Chem. Phys.*, 2009, **356**, 98–109.
69 F. Neese, *Wiley Interdiscip. Rev.: Comput. Mol. Sci.*, 2012, **2**, 73–78.
70 D. A. Pantazis, M. Orio, T. Petrenko, S. Zein, E. Bill, W. Lubitz, J. Messinger and F. Neese, *Chem. – Eur. J.*, 2009, **15**, 5108–5123.
71 D. A. Pantazis, M. Orio, T. Petrenko, S. Zein, W. Lubitz, J. Messinger and F. Neese, *Phys. Chem. Chem. Phys.*, 2009, **11**, 6788–6798.
72 W. Ames, D. A. Pantazis, V. Krewald, N. Cox, J. Messinger, W. Lubitz and F. Neese, *J. Am. Chem. Soc.*, 2011, **133**, 19743–19757.
73 N. Cox, L. Rapatskiy, J.-H. Su, D. A. Pantazis, M. Sugiura, L. Kulik, P. Dorlet, A. W. Rutherford, F. Neese, A. Boussac, W. Lubitz and J. Messinger, *J. Am. Chem. Soc.*, 2011, **133**, 3635–3648.
74 J.-H. Su, N. Cox, W. Ames, D. A. Pantazis, L. Rapatskiy, T. Lohmiller, L. V. Kulik, P. Dorlet, A. W. Rutherford, F. Neese, A. Boussac, W. Lubitz and J. Messinger, *Biochim. Biophys. Acta, Bioenerg.*, 2011, **1807**, 829–840.
75 V. Krewald, F. Neese and D. A. Pantazis, *J. Am. Chem. Soc.*, 2013, **135**, 5726–5739.
76 M. Pérez Navarro, W. M. Ames, H. Nilsson, T. Lohmiller, D. A. Pantazis, L. Rapatskiy, M. M. Nowaczyk, F. Neese, A. Boussac, J. Messinger, W. Lubitz and N. Cox, *Proc. Natl. Acad. Sci. U. S. A.*, 2013, **110**, 15561–15566.
77 M. Retegan, F. Neese and D. A. Pantazis, *J. Chem. Theory Comput.*, 2013, **9**, 3832–3842.
78 F. Neese, *J. Chem. Phys.*, 2001, **115**, 11080–11096.
79 F. Neese, *J. Chem. Phys.*, 2005, **122**, 034107.

80 L. D. Slep, A. Mijovilovich, W. Meyer-Klaucke, T. Weyhermüller, E. Bill, E. Bothe, F. Neese and K. Wieghardt, *J. Am. Chem. Soc.*, 2003, **125**, 15554–15570.
81 Y. Umena, K. Kawakami, J.-R. Shen and N. Kamiya, *Nature*, 2011, **473**, 55–60.
82 T. Lohmiller, N. Cox, J.-H. Su, J. Messinger and W. Lubitz, *J. Biol. Chem.*, 2012, **287**, 24721–24733.
83 L. Rapatskiy, N. Cox, A. Savitsky, W. M. Ames, J. Sander, M. M. Nowaczyk, M. Rögner, A. Boussac, F. Neese, J. Messinger and W. Lubitz, *J. Am. Chem. Soc.*, 2012, **134**, 16619–16634.
84 T. Lohmiller, V. Krewald, M. Pérez Navarro, M. Retegan, L. Rapatskiy, M. M. Nowaczyk, A. Boussac, F. Neese, W. Lubitz, D. A. Pantazis and N. Cox, *Phys. Chem. Chem. Phys.*, 2014, DOI: 10.1039/C3CP55017F.
85 Y. Pushkar, J. Yano, K. Sauer, A. Boussac and V. K. Yachandra, *Proc. Natl. Acad. Sci. U. S. A.*, 2008, **105**, 1879–1884.
86 D. Bovi, D. Narzi and L. Guidoni, *Angew. Chem., Int. Ed.*, 2013, **52**, 11744–11749.
87 S. Styring, J. Sjöholm and F. Mamedov, *Biochim. Biophys. Acta, Bioenerg.*, 2012, **1817**, 76–87.
88 R. Hart and P. J. O'Malley, *Biochim. Biophys. Acta, Bioenerg.*, 2010, **1797**, 250–254.
89 K. Saito, A. W. Rutherford and H. Ishikita, *Proc. Natl. Acad. Sci. U. S. A.*, 2013, **110**, 7690–7695.
90 G. F. Moore, M. Hambourger, M. Gervaldo, O. G. Poluektov, T. Rajh, D. Gust, T. A. Moore and A. L. Moore, *J. Am. Chem. Soc.*, 2008, **130**, 10466–10467.
91 P. E. M. Siegbahn, *Phys. Chem. Chem. Phys.*, 2012, **14**, 4849–4856.
92 P. E. M. Siegbahn, *J. Am. Chem. Soc.*, 2013, **135**, 9442–9449.
93 P. E. M. Siegbahn, *Biochim. Biophys. Acta, Bioenerg.*, 2013, **1827**, 1003–1019.
94 F. M. Ho, in *Molecular Solar Fuels*, ed. T. J. Wydrzynski and W. Hillier, The Royal Society of Chemistry, Cambridge, 2012, pp. 208–248.
95 K. N. Ferreira, T. M. Iverson, K. Maghlaoui, J. Barber and S. Iwata, *Science*, 2004, **303**, 1831–1838.
96 H. Ishikita, W. Saenger, B. Loll, J. Biesiadka and E.-W. Knapp, *Biochemistry*, 2006, **45**, 2063–2071.
97 I. Rivalta, M. Amin, S. Luber, S. Vassiliev, R. Pokhrel, Y. Umena, K. Kawakami, J. R. Shen, N. Kamiya, D. Bruce, G. W. Brudvig, M. R. Gunner and V. S. Batista, *Biochemistry*, 2011, **50**, 6312–6315.
98 K. Linke and F. M. Ho, *Biochim. Biophys. Acta, Bioenerg.*, 2014, **1837**, 14–32.
99 R. J. Service, W. Hillier and R. J. Debus, *Biochemistry*, 2010, **49**, 6655–6669.
100 R. J. Service, W. Hillier and R. J. Debus, *Biochemistry*, 2014, **53**, 1001–1017.
101 M. Shoji, H. Isobe, S. Yamanaka, Y. Umena, K. Kawakami, N. Kamiya, J. R. Shen and K. Yamaguchi, *Catal. Sci. Technol.*, 2013, **3**, 1831–1848.
102 P. J. O'Malley, *J. Am. Chem. Soc.*, 1998, **120**, 11732–11737.
103 Y.-N. Wang and L. A. Eriksson, *Int. J. Quantum Chem.*, 2001, **83**, 220–229.
104 M. Engström, F. Himo, A. Gräslund, B. Minaev, O. Vahtras and H. Agren, *J. Phys. Chem. A*, 2000, **104**, 5149–5153.
105 M. Brynda and R. David Britt, *Res. Chem. Intermed.*, 2007, **33**, 863–883.
106 M. Engström, F. Himo and H. Ågren, *Chem. Phys. Lett.*, 2000, **319**, 191–196.
107 M. Kaupp, T. Gress, R. Reviakine, O. L. Malkina and V. G. Malkin, *J. Phys. Chem. B*, 2002, **107**, 331–337.
108 H. Matsuoka, J.-R. Shen, A. Kawamori, K. Nishiyama, Y. Ohba and S. Yamauchi, *J. Am. Chem. Soc.*, 2011, **133**, 4655–4660.
109 K. Saito, J.-R. Shen, T. Ishida and H. Ishikita, *Biochemistry*, 2011, **50**, 9836–9844.
110 K. Saito and H. Ishikita, *Biochim. Biophys. Acta, Bioenerg.*, 2014, **1837**, 159–166.
111 W. Hofbauer, A. Zouni, R. Bittl, J. Kern, P. Orth, F. Lendzian, P. Fromme, H. T. Witt and W. Lubitz, *Proc. Natl. Acad. Sci. U. S. A.*, 2001, **98**, 6623–6628.
112 M. Högbom, M. Galander, M. Andersson, M. Kolberg, W. Hofbauer, G. Lassmann, P. Nordlund and F. Lendzian, *Proc. Natl. Acad. Sci. U. S. A.*, 2003, **100**, 3209–3214.
113 G. Bleifuss, M. Kolberg, S. Pötsch, W. Hofbauer, R. Bittl, W. Lubitz, A. Gräslund, G. Lassmann and F. Lendzian, *Biochemistry*, 2001, **40**, 15362–15368.
114 M. R. Seyedsayamdost, T. Argirević, E. C. Minnihan, J. Stubbe and M. Bennati, *J. Am. Chem. Soc.*, 2009, **131**, 15729–15738.
115 T. Argirević, C. Riplinger, J. Stubbe, F. Neese and M. Bennati, *J. Am. Chem. Soc.*, 2012, **134**, 17661–17670.
116 L. Benisvy, R. Bittl, E. Bothe, C. D. Garner, J. McMaster, S. Ross, C. Teutloff and F. Neese, *Angew. Chem., Int. Ed.*, 2005, **44**, 5314–5317.
117 S. Sinnecker, E. Reijerse, F. Neese and W. Lubitz, *J. Am. Chem. Soc.*, 2004, **126**, 3280–3290.
118 S. Sinnecker, M. Flores and W. Lubitz, *Phys. Chem. Chem. Phys.*, 2006, **8**, 5659–5670.
119 H. J. van Gorkom and C. F. Yocum, in *Photosystem II. The Light-Driven Water: Plastoquinone Oxidoreductase*, ed. T. Wydrzynski and K. Satoh, Springer, Dordrecht, 2005, vol. 22, pp. 307–328.
120 C. F. Yocum, *Coord. Chem. Rev.*, 2008, **252**, 296–305.
121 M. Miqyass, H. J. Gorkom and C. F. Yocum, *Photosynth. Res.*, 2007, **92**, 275–287.
122 B. C. Polander and B. A. Barry, *J. Phys. Chem. Lett.*, 2013, 786–791.
123 F. Rappaport, N. Ishida, M. Sugiura and A. Boussac, *Energy Environ. Sci.*, 2011, **4**, 2520–2524.
124 E. Y. Tsui, R. Tran, J. Yano and T. Agapie, *Nat. Chem.*, 2013, **5**, 293–299.
125 T. Irebo, S. Y. Reece, M. Sjödin, D. G. Nocera and L. Hammarström, *J. Am. Chem. Soc.*, 2007, **129**, 15462–15464.